A Reduced Transport Model for Ion Heat Diffusivity by Gyro-Kinetic Analysis with Kinetic Electrons in Helical Plasmas

Shinichiro TODA, Motoki NAKATA, Masanori NUNAMI, Akihiro ISHIZAWA[1)],
Tomo-Hiko WATANABE[2)] and Hideo SUGAMA

National Institute for Fusion Science, 322-6 Oroshi-cho, Toki, Gifu 509-5292, Japan
[1)]*Graduate School of Energy Science, Kyoto University, Gokasho, Uji, Kyoto 611-0011, Japan*
[2)]*Department of Physics, Nagoya University, Furo-cho, Nagoya, Aichi 464-8602, Japan*

A high ion temperature plasma in the Large Helical Device is examined in the case in which the ion temperature gradient mode is unstable. The nonlinear gyro-kinetic simulation is performed to evaluate the turbulent ion heat diffusivity with the kinetic electron response. It is clarified that the decay time of zonal flows [S. Ferrando-Margalet *et al.*, Phys. Plasmas **14**, 122505 (2007)] decreases radially outward due to the trapped electron and the ion energy transport increases outward. To reduce the computational cost for applying to the dynamical transport simulation, an extended transport model for the ion heat diffusivity in terms of the mixing length estimate and the characteristic quantity for the linear response of zonal flows is proposed.

Turbulent transport is one of the most critical issues for plasma confinement in magnetic fusion devices. Theoretical expressions for the turbulent transport due to the various instabilities were reviewed [1]. Recently, a large number of the gyro-kinetic simulations which are applied to the turbulent transport have been performed in toroidal plasmas, *e.g.* [2–8]. The gyro-kinetic analysis results in tokamak [9–11] and helical [12–14] plasmas have been studied with the experimental observations. Gyro-kinetic simulations of helical plasmas require a large number of mesh points along the field line in order to capture the helical ripple structure. Therefore, the gyro-kinetic analysis in helical plasmas consumes the larger computer resources than for tokamaks. In helical plasmas, it is not practical to perform the nonlinear gyro-kinetic simulation at each time step of the dynamical transport code. The reduced model, which reproduces the nonlinear gyro-kinetic analysis results, is needed for the dynamical transport simulation in helical plasmas.

The GKV code [15] has been used to examine the ion temperature gradient (ITG) mode and zonal flows in the Large Helical Device (LHD) for studying the turbulent transport [13]. The gyro-kinetic simulation with the adiabatic electron is performed for the high ion temperature LHD discharge (shot number 88343 [16]). The ion energy flux by the ITG mode instability agrees with the experimental results [13, 14]. The reduced model for the ion heat diffusivity is proposed [14] by the simulation with the adiabatic electron. This reduced model is the function of the

linear growth rate for the ITG mode and the zonal flow decay time [17, 18]. In tokamak plasmas, the gyro-kinetic analysis at each time step is globally performed in the dynamical transport simulation [19, 20]. How to apply the reduced model of the turbulent ion heat diffusivity from the gyro-kinetic simulation with the adiabatic electron to the transport code has been shown in helical plasmas [21]. The simulation with the kinetic electron shows the larger ion energy flux than the experimental results in the high-T_i LHD discharge [22]. On the other hand, the electron and ion energy fluxes of the simulation results with the kinetic electron are close to those of the experimental results in the low-T_i #88343 discharge [23]. The simulation result with the adiabatic electron in this low-T_i discharge shows that the ITG mode becomes stable around $\rho(= r/a) = 0.5$. The effect of the kinetic electron induces the enhancement of the linear growth rate of ITG modes [4,22]. To show the reduced transport model for the turbulent ion heat diffusivity, the effect of the kinetic electron on the plasma instability should be included.

In this study, the reduced model of the ion heat diffusivity for the ITG mode is proposed by solving the gyro-kinetic equation in terms of the electron in addition to the ion to examine the effect of the kinetic electron. The same method with the gyro-kinetic analysis using the adiabatic electron [14] is adopted. The nonlinear gyro-kinetic simulation is performed to evaluate the ion heat diffusivity. The effect of the kinetic electron on the linear response of zonal flows is studied. The linear gyro-kinetic simulation is also performed for the reduced model in order to reproduce the
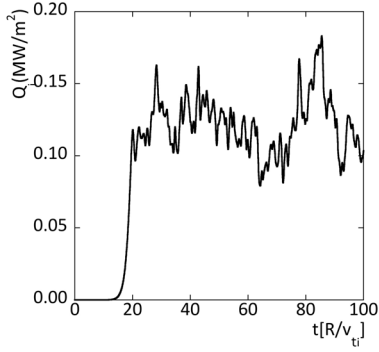
Fig. 1   Time evolution of the ion energy flux.

value of the ion heat diffusivity by the nonlinear analysis.

We examine the turbulence driven by the microinstabilities in LHD plasmas, using the gyro-kinetic local flux tube code GKV [15]. Based on the temperatures radial profiles, density radial profiles, and field configuration from the LHD experimental results of the high-T_i phase at $t = 2.233$ s [16], the electron and ion temperature gradients, R/L_{T_e} and R/L_{T_i}, the density gradient R/L_n, and the safety factor q radially change. The GKV simulation with the kinetic electron is performed with $R = 3.75$ m. The $\beta(= 2\mu_0 n(T_e + T_i)/B^2)$ value is 0.3% at $\rho = 0.65$. To reduce computer resources and perform the nonlinear analysis in the wide plasma parameter region, we take the smaller number for the Fourier modes and the smaller number of the grid points in this simulation than in the case in [22]. The total Fourier mode numbers in the $\tilde{k}_x$ and $\tilde{k}_y$ directions are 9 and 6 in the regions $-0.5 \leq \tilde{k}_x \leq 0.5$ and $0.0 \leq \tilde{k}_y \leq 0.5$, where $\tilde{k}_x(= k_x\rho_i)$ and $\tilde{k}_y(= k_y\rho_i)$ are the radial and poloidal wavenumbers. The nonlinear GKV simulations are carried out at ten radial points between $\rho = 0.46$ and $\rho = 0.80$. As an example, the time evolution of the ion energy flux Q_i at $\rho = 0.65$ is shown in Fig. 1. The value of time t is normalized by R/v_{ti}. The saturation of the ion energy flux is obtained in the nonlinear phase. The averaged value of the ion energy flux in the time interval $50 < t < 100$ is 0.12 MW/m². In [22], the averaged value of the ion energy flux in the time interval $50 < t < 80$ is about 0.13 MW/m², when the Fourier mode numbers in the $\tilde{k}_x$ and $\tilde{k}_y$ directions are 169 and 43. Even if the number of the Fourier modes is small, the close value of the ion energy flux is obtained in this study. This is because the peaks of the electrostatic potential fluctuation are found in the regions $0.0 \leq \tilde{k}_{x,y} \leq 0.5$ and the values of the electrostatic potential fluctuation in the regions $\tilde{k}_{x,y} > 1.0$ are extremely small. The averaged value of the ratio of the electromagnetic contribution Q_i^{em} to the total ion energy flux Q_i in the time interval $50 < t < 100$ is 0.33%, because of the low beta 0.3% plasma. The finite beta effect is negligibly small to the ion electrostatic flux in this study. The values of $\bar{\chi}_i$ by the simulation with the kinetic electron are from two to three times larger than those by the simulation

Table 1   Parameter region in the nonlinear simulations.

ρ	0.46 to 0.80
q	1.3 to 2.2
R/L_{T_i}	6.6 to 16
R/L_{T_e}	4.6 to 15
R/L_n	-1.0 to 1.7
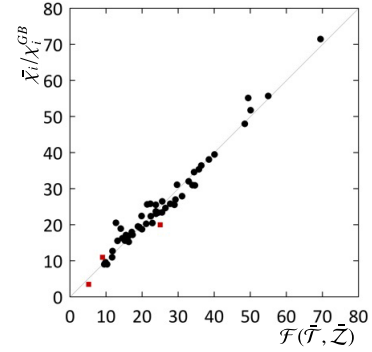
Fig. 2   Comparison of $\bar{\chi}_i/\chi_i^{GB}$ from the nonlinear gyro-kinetic simulation with the model function $\mathcal{F}(\bar{\mathcal{T}}, \bar{\mathcal{Z}})$. The circles and the boxes show the results in high-T_i and low-T_i phases.

with the adiabatic electron. The bar ¯ shows the averaged value in the time interval of the nonlinear saturation phase. The time evolutions of the squared turbulent potential fluctuation, $\mathcal{T}\left(= \Sigma_{\tilde{k}_x,\tilde{k}_y\neq0} \left\langle \left|\tilde{\phi}_{\tilde{k}_x,\tilde{k}_y}\right|^2 \right\rangle /2\right)$ and the squared zonal flow potential, $\mathcal{Z}\left(= \Sigma_{\tilde{k}_x} \left\langle \left|\tilde{\phi}_{\tilde{k}_x,\tilde{k}_y=0}\right|^2 \right\rangle /2\right)$ are studied, where $\tilde{\phi}$ is the electrostatic potential fluctuation which is defined as $\tilde{\phi} = \phi/(T_i\rho_i/(eR))$. The bracket $\langle\rangle$ denotes the averaged values along the magnetic field line. The nonlinear saturation is seen in the time evolution of $\mathcal{T}$ and $\mathcal{Z}$.

The normalized electron and ion temperature gradients are artificially altered at 0.8 and 1.2 times the experimental values at ten radial points. This is because the ion energy flux decreases with the reduced gradient by 20% and close to the experimental value [22]. The parameter range in which the nonlinear simulation has been performed is shown in Table 1. The transport coefficients $\bar{\chi}_i/\chi_i^{GB}$ by the nonlinear simulation are compared with a model function of $\bar{\mathcal{T}}$ and $\bar{\mathcal{Z}}$ by the circles in Fig. 2. A fitting function for the ion heat diffusivity is defined by

$$\frac{\bar{\chi}_i}{\chi_i^{GB}} = \mathcal{F}(\bar{\mathcal{T}}, \bar{\mathcal{Z}}) \equiv \frac{C_1\bar{\mathcal{T}}^\alpha}{C_2 + \bar{\mathcal{Z}}^{\frac{1}{2}}/\bar{\mathcal{T}}}, \qquad (1)$$

with $\alpha = 0.46$, $C_1 = 5.5\times10^{-2}$, and $C_2 = 2.2\times10^{-2}$, where χ_i^{GB} is the gyro-Bohm diffusivity. The relative error for fitting $\bar{\chi}_i/\chi_i^{GB}$ by $\mathcal{F}$ is 0.12, where the relative error is defined as the root mean square of $\left[(\bar{\chi}_i/\chi_i^{GB})/\mathcal{F} - 1\right]$. The value of the ion heat diffusivity is well reproduced by the model function (1). The values of the coefficients, α, C_1, and

C_2 in this article are similar to those of the coefficients by the simulation with the adiabatic electron [14]. In [23], the gyro-kinetic simulation is performed in the low-T_i phase for #88343 in the LHD. The values of the normalized ion heat diffusivity by the model (1) are comparable with the values by the nonlinear simulation at three radial points in the low-T_i phase [23] with the boxes in Fig. 2.

To represent the contributions of the turbulent fluctuations and zonal flow fluctuations to the turbulence level by the linear gyro-kinetic analysis, the simulation is performed with the kinetic electron. The values of the linear growth rate by the simulation with the kinetic electron are several times larger than those by the simulation with the adiabatic electron. The instabilities are driven by the ITG mode because the real frequency is negative and the mode rotates towards the ion diamagnetic direction. Figure 3 shows the relation between the turbulence fluctuation $\bar{\mathcal{T}}$ and the mixing length estimate $\mathcal{L} \left(\equiv \int (\tilde{\gamma}_{\tilde{k}_y}/\tilde{k}_y^2) d\tilde{k}_y \right)$ [24] integrated over $0.1 \leq \tilde{k}_y \leq 0.5$ with the circles, where $\tilde{\gamma}_{\tilde{k}_y} (= \gamma_{\tilde{k}_y}/(v_{ti}/R))$ is the linear growth rate. The turbulence fluctuation $\bar{\mathcal{T}}$ is approximated by

$$\bar{\mathcal{T}} = C_T \mathcal{L}^a, \tag{2}$$

with the coefficients $C_T = 4.8 \times 10$ and $a = 2.1$. The three values of $\bar{\mathcal{T}}$ by the nonlinear simulation in the low-T_i phase are found to be comparable with those by Eq. (2) with the boxes in Fig. 3. The turbulent transport level is not only determined by the mixing length estimate. The level of the turbulence is also determined by the interaction between the turbulence and the zonal flows shown in Eq. (1). The linear zonal flow response function is defined by $\mathcal{R}_{\tilde{k}_x}(t) \equiv \left\langle \tilde{\phi}_{\tilde{k}_x, \tilde{k}_y=0}(t) \right\rangle / \left\langle \tilde{\phi}_{\tilde{k}_x, \tilde{k}_y=0}(t = 0) \right\rangle$. We examine the linear zonal flow response using the field configuration for the high-T_i and low-T_i phases in the LHD #88343 discharge. In the low-T_i phase, the magnetic field configuration is shifted inward and the major radius is close to 3.6 m. In the inward shifted field configuration, the helical magnetic structure can enhance the generation of zonal flows [25]. The linear zonal flow response depends on the mag-

netic field configuration but does not depend on the plasma profile. Note that we set the value of $\tilde{k}_x$ around 0.25, because there is a peak of the wavenumber spectra around $\tilde{k}_x = 0.25$ as the results of the nonlinear simulation. To examine the correlation between $\mathcal{R}_{\tilde{k}_x}(t)$ and the fluctuation of zonal flows $\bar{\mathcal{Z}}$, the zonal flow decay time [18] is employed. The zonal flow decay time is defined by $\tau_{ZF} \equiv \int_0^{\tau_f} dt \mathcal{R}_{\tilde{k}_x}(t)$, where τ_f is the upper limit of t in the integral. Here, we set $\tau_f = 15R/v_{ti}$, because the zonal flow decay time does not change significantly for $\tau_f > 15R/v_{ti}$. The correlation time of the turbulence in the nonlinear simulation result shown in Fig. 1 is shorter than $15R/v_{ti}$, thus $\mathcal{R}_{\tilde{k}_x}(t)$ for $\tau_f > 15R/v_{ti}$ does not influence the excited zonal flow level. The zonal flow fluctuation $\bar{\mathcal{Z}}$ is approximated by the linear simulation results as the function of $\tilde{\tau}_{ZF}(= \tau_{ZF}/(R/v_{ti}))$ and $\bar{\mathcal{T}}$,

$$\bar{\mathcal{Z}} = C_z \tilde{\tau}_{ZF}^b \bar{\mathcal{T}}^c, \tag{3}$$

with $C_z = 0.0061$, $b = 1.6$ and $c = 1.4$. The comparison of $\bar{\mathcal{Z}}$ with $0.0061 \tilde{\tau}_{ZF}^{1.6} \bar{\mathcal{T}}^{1.4}$ is shown in Fig. 4. The circles and boxes represent the simulation results in the high-T_i and low-T_i phases.

We study the difference of the linear zonal flow response with the kinetic electron from that with the adiabatic electron. Figure 5 represents the time trace of the lin-
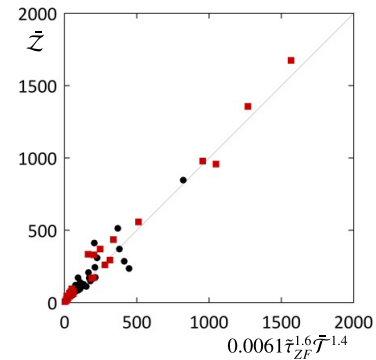
Fig. 4 The plots for the comparison of $\bar{\mathcal{Z}}$ with $0.0061 \tilde{\tau}_{ZF}^{1.6} \bar{\mathcal{T}}^{1.4}$. The circles show the simulation results in the high-T_i phase and the boxes represent those in the low-T_i phase.

Fig. 3 Comparison of the time-averaged turbulent fluctuation $\bar{\mathcal{T}}$ with the mixing length estimate, $\mathcal{L}$. The circles and the boxes represent the results in high-T_i and low-T_i phases.
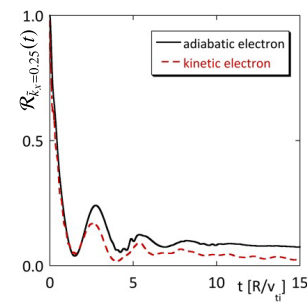
Fig. 5 Time trace of $\mathcal{R}_{\tilde{k}_x=0.25}(t)$ as the results with the adiabatic electron (solid curve) and with the kinetic electron (dashed curve) at $\rho = 0.80$.
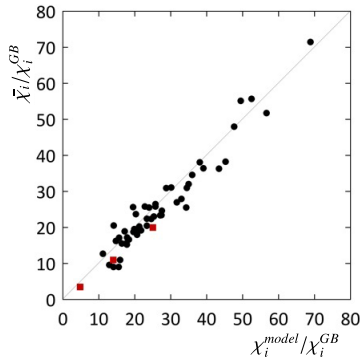
Fig. 6   The comparison of the nonlinear simulation results with the kinetic electron, $\bar{\chi}_i$ with the model predictions of Eq. (4), χ_i^{model}. The circles and the boxes show the results in high-T_i and low-T_i phases.

ear zonal flow response function $\mathcal{R}_{\tilde{k}_x}(t)$ for the simulation results with the adiabatic electron (the solid curve) and the kinetic electron (the dashed curve) at $\rho = 0.80$. The linear zonal flow response function with the kinetic electron decays faster than that with the adiabatic electron. The zonal flow decay time decreases radially outward due to the trapped electron [17]. The turbulence fluctuation $\bar{\mathcal{T}}$ increases outward. Therefore, the ion energy flux is found to increase radially outward in this study and in [23]. In the adiabatic electron case, the zonal flow decay time increases outward and the ion energy transport decreases outward [14].

When we substitute Eqs. (2) and (3) into Eq. (1), the reduced model which represents the ion heat diffusivity in terms of the linear plasma parameters by the simulation with the kinetic electron is shown as

$$\frac{\chi_i^{model}}{\chi_i^{GB}} = \frac{A_1 \mathcal{L}^{B_1}}{A_2 + \tilde{\tau}_{ZF}^{B_2}/\mathcal{L}^{B_3}}, \qquad (4)$$

where the coefficients are given by $A_1 = C_1 C_T^{\alpha+1-c/2} C_z^{-1/2} = 1.3 \times 10^1$ and $A_2 = C_2 C_T^{1-c/2} C_z^{-1/2} = 0.90$. The exponents are also given by $B_1 = \alpha a = 0.97$, $B_2 = b/2 = 0.80$, and $B_3 = a(1 - c/2) = 0.63$. By the linear gyro-kinetic simulation, the value of χ_i^{model} is obtained. The ion heat diffusivities χ_i^{model} and $\bar{\chi}_i$ are compared with the circles in Fig. 6. The reduced model reproduces the nonlinear simulation results $\bar{\chi}_i$ for the relative error 0.16. The values of the ion heat diffusivity by the reduced model (4) are comparable with those by the nonlinear simulation at three radial points in the low-T_i phase [23] with the boxes in Fig. 6.

In summary, the gyro-kinetic simulation with the kinetic electron is performed to show the reduced transport model for the turbulent ion heat diffusivity. At first, the ion heat diffusivity is evaluated from the nonlinear simulation for high-T_i plasma in the LHD, where the ITG mode is destabilized. To investigate the wide plasma parameter region, the smaller number of Fourier modes is taken than

the case in [22]. The model function for the ion heat diffusivity is shown in terms of $\bar{\mathcal{T}}$ and $\bar{\mathcal{Z}}$. Next, the terms $\bar{\mathcal{T}}$ and $\bar{\mathcal{Z}}$ in the model function are approximated by the terms of the mixing length estimate and the zonal flow decay time evaluated from the linear simulation. The use of the linear simulation results enables us to reproduce the nonlinear simulation results by the reduced model. The decay of zonal flows with the kinetic electron becomes faster. The decay time of zonal flows is found to decrease radially outward and the ion energy transport increases outward due to the trapped electron. The dependence of the reduced model for the turbulent diffusivity on the field configuration (*e.g.*, for low-T_i phase) and the plasma profiles for the LHD and different devices has been investigated. The model functions for the turbulent heat and particle diffusivities were shown in the tokamak plasmas [26]. In this study, the time averaged value in the nonlinear saturation phase of the ratio of the electromagnetic contribution to the total electron energy flux becomes about 30%, despite the low beta plasma. If the larger number of the modes is taken, the electromagnetic energy flux becomes smaller in the total electron energy flux [22]. The reduced transport models for the electron heat diffusivity and the particle diffusivity in addition to ion heat diffusivity will be studied.

[1] J.W. Connor and H.R. Wilson, Plasma Phys. Control. Fusion **36**, 719 (1994).
[2] X. Garbet *et al.*, Nucl. Fusion **50**, 0433002 (2010).
[3] F. Jenko and W. Dorland, Plasma Phys. Control. Fusion **43**, A141 (2001).
[4] J. Candy and R.E. Waltz, J. Comput. Phys. **186**, 545 (2003).
[5] T.-H. Watanabe, H. Sugama and S. Ferrando-Margalet, Nucl. Fusion **47**, 1383 (2007).
[6] P. Xanthopoulos *et al.*, Phys. Rev. Lett. **99**, 035002 (2007).
[7] M. Nunami *et al.*, Plasma Fusion Res. **6**, 1403001 (2011).
[8] A. Ishizawa *et al.*, Phys. Plasmas **21**, 055905 (2014).
[9] M. Kotschenreuther *et al.*, Phys. Plasmas **2**, 2381 (1995).
[10] C. Holland *et al.*, Phys. Plasmas **18**, 056113 (2011).
[11] T.L. Rhodes *et al.*, Nucl. Fusion **51**, 063022 (2011).
[12] H.E. Mynick, N. Pomphrey and P. Xanthopoulous, Phys. Rev. Lett. **105**, 0950094 (2010).
[13] M. Nunami *et al.*, Phys. Plasmas **19**, 042504 (2012).
[14] M. Nunami, T.-H. Watanabe and H. Sugama, Phys. Plasmas **20**, 092307 (2013).
[15] T.-H. Watanabe and H. Sugama, Nucl. Fusion **46**, 24 (2006).
[16] K. Tanaka *et al.*, Plasma Fusion Res. **5**, S2053 (2010).
[17] H. Sugama and T.-H. Watanabe, Phys. Plasmas **13**, 012501 (2006).
[18] S. Ferrando-Margalet, H. Sugama and T.-H. Watanabe, Phys. Plasmas **14**, 122505 (2007).
[19] J. Candy *et al.*, Phys. Plasmas **16**, 060704 (2009).
[20] M. Barnes *et al.*, Phys. Plasmas **17**, 056109 (2010).

[21] S. Toda *et al.*, J. Phys.: Conf. Ser. **561**, 012020 (2014).
[22] A. Ishizawa *et al.*, Nucl. Fusion **55**, 043024 (2015).
[23] A. Ishizawa *et al.*, Nucl. Fusion **57**, 066010 (2017).
[24] J. Wesson, *Tokamaks*, 2nd ed. (Oxford University Press, 1997) p.198.
[25] T.-H. Watanabe, H. Sugama and S. Ferrando-Margalet, Phys. Rev. Lett. **100**, 195002 (2008).
[26] M. Nakata *et al.*, 25th IAEA Fusion Energy Conference 13-18 Oct. St. Petersburg, Russian Federation, TH/P-38 (2014).